applied sciences

MDPI

Article

Effect of Entrance Flood Barriers on Evacuation Performance in Underground Subway Stations

Chi Yeong Kang [1], Jaehyun Shin [1,*] and Dong Sop Rhee [2,*]

[1] Department of Civil and Environmental Engineering, Gachon University, Seongnam 13120, Gyeonggi-do, Republic of Korea; kangjja9219@gachon.ac.kr
[2] Korea Institute of Civil Engineering and Building Technology, 283, Goyangdae-ro, Ilsanseo-gu, Goyang-si 10223, Gyeonggi-do, Republic of Korea
* Correspondence: jaehyunshin@gachon.ac.kr (J.S.); dsrhee@kict.re.kr (D.S.R.)

Abstract

Flood barriers at subway entrances can affect inundation through an underground station and influence the conditions encountered during evacuation. This study conducts a three-dimensional flood simulation with evacuation analysis to evaluate these effects in an idealized three level subway station. Flood inundation was simulated using OpenFOAM for six configurations with zero to three flood barriers for four entrances. Water depth and depth-averaged velocity were converted into pedestrian walking speed retention factors. The evacuation routing model was based on Dijkstra's algorithm, with each evacuation link assigned a travel time cost based on link length, normal walking speed, flood induced speed reduction, and crowd congestion effects. The hydraulic results showed spatially heterogeneous mobility reduction, with concentrated flow along inter-floor stairways. The estimated maximum evacuation time was 574 s without barriers and decreased to 542 s, 468–487 s and 399–400 s with one, two and three barriers, respectively. The first barrier reduced the evacuation time by 5.6%, whereas two and three barriers reduced it by 15.2–18.5% and 30.3–30.5%, showing that the effect of barriers was not proportional to their number. The benefit of flood barriers appeared as a change in walking speed rather than as a change in route. These results show the effect of entrance protection through its effects on local pedestrian mobility and station evacuation.

Keywords: flood simulation; evacuation simulation; Dijkstra's algorithm; OpenFOAM; underground subway station

Check for updates

Academic Editor: Peng Hou

Received: 27 October 2026
Revised: 19 November 2026
Accepted: 24 November 2026
Published: 26 November 2026

Copyright: © 2026 by the authors. Licensee MDPI, Basel, Switzerland. This article is an open access article distributed under the terms and conditions of the Creative Commons Attribution (CC BY) license.

1. Introduction

Underground subway stations are particularly vulnerable to urban flooding because their configuration allows surface runoff to enter through station entrances and propagate rapidly toward lower floors through corridors, stairways, and escalators. Once floodwater enters the station, the connections heading underground such as stairs and escalators can become major hydraulic pathways and critical evacuation routes, creating a direct conflict between flood propagation and pedestrian safety. Previous research has shown that flooding can reduce pedestrian walking speed and alter the accessibility of evacuation routes as water depth and flow velocity increase. Structural countermeasures such as entrance flood barriers may therefore influence not only the amount of water entering the station but also the availability and efficiency of evacuation pathways. Accordingly, evaluating flood control measures requires an integrated approach that considers three-dimensional flood

behavior, pedestrian mobility, and evacuation route selection under different flood barrier operating scenarios.

Numerical modeling has been widely employed to investigate flood propagation in underground spaces because direct measurements and observations during actual subway inundation events are difficult to obtain and generally provide limited information on spatial variations in water depth and flow velocity. Former studies commonly employed depth-averaged approaches because of their computational efficiency. Son et al. [1] subsequently coupled a one-dimensional SWMM drainage model with a two-dimensional overland flow model and proposed boundary and pond type approaches for representing the transfer of surface floodwater into underground spaces. More recently, multilayer shallow water frameworks have been extended to improve the representation of momentum transfer through stairways and to support evaluation of flood control barriers in multilevel underground stations [2]. Numerical simulations were conducted for analysis of flood dynamics over various types of staircases in underground spaces with changes to shorter or higher steps and examined effects to hazard degree for pedestrian stability [3]. These approaches provide efficient tools for large scale or preliminary flood risk assessment, but the simplification of vertical connections can limit the representation of three-dimensional hydraulic processes around stairways and landings.

Accordingly, three-dimensional computational fluid dynamics has increasingly been adopted when detailed local hydraulic information is required. OpenFOAM was used to reproduce inundation within a subway-station model and showed that three-dimensional simulations can resolve spatial variations in water depth, velocity, and pedestrian oriented flood risk indices [4]. Lu et al. [5] similarly applied CFD with a VOF model to simulate the complete flood-invasion process in a subway station under different entrance water levels and analyzed temporal changes in flood propagation and tunnel inflow. Wang et al. [6] developed a three-dimensional subway flood-intrusion model based on the realizable k-e turbulence model and VOF method and investigated the influence of floodgate operation, the number of active water inlets, and inlet water depth. Li et al. [7] used the LES model to simulate flow characteristics and fluid-human interactions in staircases to analyze the sliding instability to child and adult models. Collectively, these studies indicate a tradeoff between the computational efficiency of depth-averaged or multilayer models and the detailed hydraulic information available from 3D CFD. Since the present study aims to connect local flood depth and velocity around floors and stairways directly to pedestrian walking speed reduction and evacuation routing, a three-dimensional OpenFOAM framework was adopted to provide spatially resolved hydraulic inputs for the evacuation model.

Evacuation modeling for underground stations has generally followed one of two approaches. Microscopic models such as the social force model [8] and its variants [9] reproduce individual pedestrian trajectories and are effective for analyzing local bottlenecks, but their computational cost grows rapidly with population size and network extent, which limits their use for multi-level stations with several thousand occupants. Network-based approaches address this by abstracting the station into a graph of nodes and links and solving the routing problem with a shortest-path algorithm, most commonly Dijkstra's algorithm [10], which guarantees the globally shortest path on a non-negatively weighted graph and can be re-executed whenever link costs change. Such models have been applied to subway station evacuation [11], real-time building evacuation guidance [12], and multi-modal cooperative guidance in metro stations [13], and have been extended to hazard-specific settings including tailings dam failure [14] and earthquake evacuation [15]. For deep underground stations, node–link models have been used to identify optimal additional evacuation routes [16], to evaluate fire evacuation efficiency under dynamic crowd and smoke conditions [17], and to allocate evacuees to exits in a system-optimal manner [18].

Where flooding is concerned, most existing work has examined the physical limits of pedestrian movement in inundated staircases [19] or has combined an inundation map with pre-defined escape routes for risk assessment [20], rather than treating the flood as a factor that changes the walking speed on every link and therefore the route itself. In particular, the effect of entrance flood barriers on evacuation performance, acting through the reduction of inflow and the resulting change in walking conditions inside the station, has not been evaluated.

The objective of this study is to evaluate how entrance flood barrier configurations influence pedestrian mobility and evacuation performance in a multilevel underground subway stations. Unlike simplified inundation models, the present study conducts a three-dimensional numerical simulation with OpenFOAM to simulate water flow through interconnected underground floors. Six flood barrier scenarios are considered, corresponding to 0, 1, 2, and 3 closed barriers to stop flood entering through each section. The resulting spatial distributions of water depth and flow velocity are then converted into flood induced pedestrian walking speed reduction factors. Dijkstra's algorithm is used to determine minimum travel time evacuation routes while accounting for both hydraulic conditions and crowd related movement constraints. These results will be incorporated into time dependent evacuation link costs, and comparisons of evacuation times and route changes will be analyzed on how the hydraulic benefits of entrance protection influence station clearance. The resulting evacuation routes, evacuation time, and route changes will be compared across the six flood barrier scenarios.

2. Methodology

2.1. Spatial Modeling

The methodology for this research consists of sequential modeling using three-dimensional hydraulic simulation and evacuation-route optimization. First, a three-dimensional representation of the underground station is constructed, including three basement levels, four surface entrances, horizontal platform and concourse areas, and the stairway connections between adjacent floors. Simulated hydraulic variables from the three dimensional configuration were converted into spatial-averaged pedestrian walking speed reduction factors before being applied to evacuation network link weights. As for this research the information is obtained from fully three-dimensional CFD OpenFOAM simulation results rather than storage–link inundation networks.

An idealized three level underground subway station is employed as the computational domain to investigate the interaction between flooding, flood barrier operation, and pedestrian evacuation. The station consists of three primary underground levels designated with the B1 as the exit level, B2 as the concourse, and B3 as the platform with an outlet. An idealized layout was used so that barrier configurations could be compared under otherwise identical conditions. A generic geometry avoids site-specific features that would obscure the effect of the barriers. Detailed design drawings of a real subway station were not available so the geometry does not reproduce an actual existing station. The model includes geometric simplifications so the simulated flow, evacuation times, and the governing exit depend on the assumed floor area and positions of the stairways and entrances.

The horizontal computational domain is approximately 50 m × 50 m, while the three accessible floor levels for pedestrians are vertically separated and connected through multiple stairways as shown in Figure 1. Four surface entrances are positioned around the outer boundary of the B1 level. Each open entrance serves as a potential floodwater inflow boundary, and six hydraulic scenarios therefore represent progressively increasing levels of flood protection, starting with no flood barrier used, to three flood barriers installed. Vertical connectivity is provided by four stairways between B1 and B2 and six stairways between

B2 and B3. These connections are explicitly represented as inclined three-dimensional geometries rather than equivalent hydraulic links for the three-dimensional flood simulation. Their locations are also within the evacuation network because the same stairways serve as critical pedestrian movement links between floors.

Six hydraulic scenarios were considered according to the number of operational flood barriers. The first 0-closed flood barrier scenario represents the baseline case in which all four entrances are open and floodwater can enter through E1–E4. The 1-closed flood barrier scenario contains one protected entrance E1 and three open entrances. The 2-closed flood barrier scenario contains two protected entrances E1 and E3, with another case E2 and E4 protected for comparison. The 3-closed flood barrier scenario represents the highest level of protection, with only one entrance E4, or E1 for a comparing case permitting inflow. Each case therefore represents a progressively reduced number of surface inflow pathways by flood barriers. These cases were compared to determine whether reducing the number of entrances admitting floodwater leads to proportional improvements in underground hydraulic conditions. The comparison also examined whether station geometry and stairway connections produce nonlinear effects on flood propagation and evacuation safety.

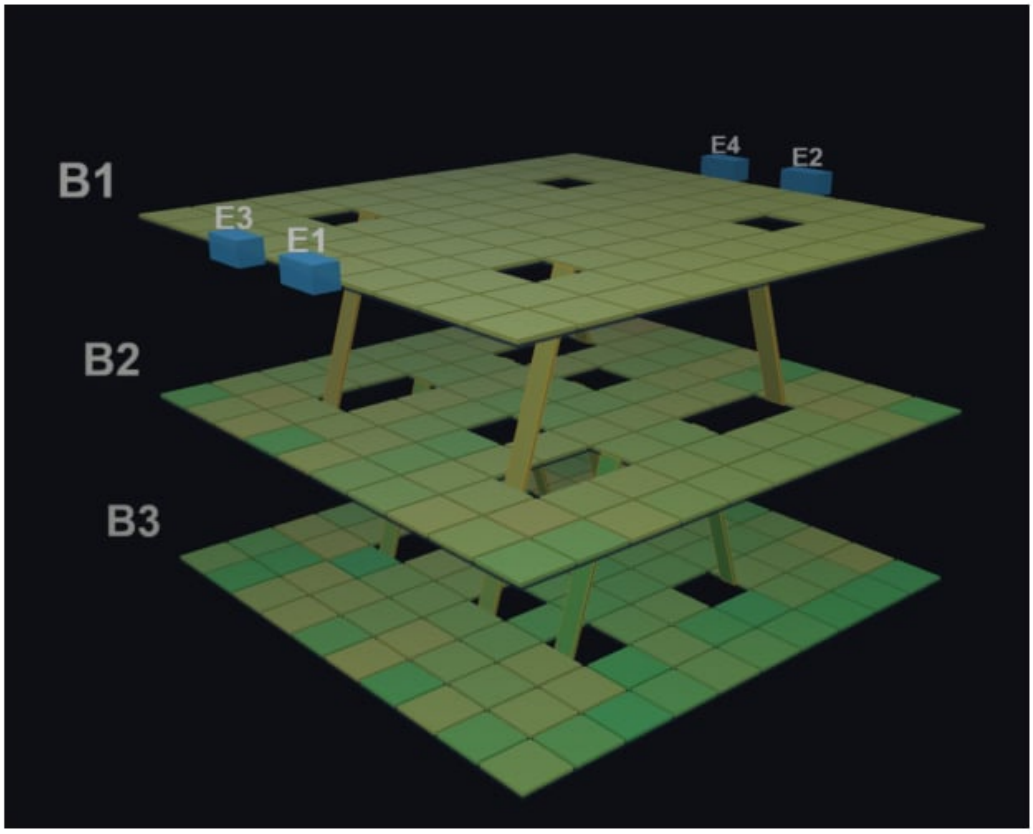

Figure 1. Layout of underground subway station.

2.2. Initial Occupant Distribution

The number of occupants present in the station at the onset of flooding was determined from the ridership statistics of the target station provided by the Seoul Metropolitan Government. The peak 30-min boarding volume of the Sillim Line at this station, 3974 passengers, was adopted as the total evacuee population. Using the boarding volume rather than a cross-sectional passenger count gives a conservative estimate that represents the most crowded period of the day, and the same population was applied to all cases so that differences in evacuation performance can be attributed to the flood barrier configuration

alone. The boarding volume accumulates over 30 min, whereas the number of passengers simultaneously present in the station is approximately the boarding rate multiplied by the average time spent in the station, so the adopted population is an upper bound rather than a typical occupancy. The ridership statistics were used only to load the network with a realistic peak population; the station geometry is idealized and is not intended to reproduce the layout of this station.

Because the study addresses the moment at which surface water begins to enter the station rather than the instant of train arrival, occupants were assumed to be present on both the platform level (B3) and the concourse level (B2). The population was divided between the two levels in a 7:3 ratio, giving 2782 occupants on the platform and 1192 in the concourse; this ratio reflects the proportion of passengers waiting on the platform relative to those moving through the fare-gate and concourse areas during the peak period. No occupants were assigned to the exit level (B1), which serves only as the connection between the station and the four surface entrances E1–E4. The resulting allocation is summarized in Table 1.

Table 1. Initial occupant distribution over the node–link network.

Level	Area	Node Group	Number of Nodes	Occupants per Node	Subtotal	Share of Total
B3	Platform	Group P1 Group P2	82 18	28 27	2782	70%
B2	Concourse	Group C1 Group C2	42 8	24 23	1192	30%
B1	Exit level	–	–	0	0	0%
Total			150 (loaded)		3974	100%

On the platform level, occupants were distributed over all 100 platform nodes so that the entire platform area is loaded, as it would be while passengers wait for a train. On the concourse level, where passengers are spread unevenly between the paid area, the fare gates and the passageways, occupants were assigned to a randomly selected half of the 100 concourse nodes, leaving the remainder empty. Within each level the population was first divided equally among the target nodes, and the remainder after integer division was added one person at a time to a subset of those nodes so that the total matches the statistical value exactly. This gives 28 occupants on 82 platform nodes and 27 on the remaining 18, and 24 occupants on 42 concourse nodes and 23 on the remaining 8. For the 5 m × 5 m nodal area this corresponds to approximately 1.1 persons/m^2 on the platform and 0.9–1.0 persons/m^2 on the loaded concourse nodes, a moderately crowded but not saturated condition consistent with a light-rail platform during peak hours. The spatial distribution of the initial population over the node–link network is shown in Figure 2.

2.3. Inundation Simulation Model

Three-dimensional flooding movement within the underground station was simulated using OpenFOAM, an open source computational fluid dynamics framework capable of resolving transient multiphase free surface flows. The interFoam solver was employed to represent the simultaneous presence of water and air using the Volume of Fluid (VOF) method. In this formulation, the water volume fraction is transported throughout the computational domain, using cells which represent the percent of water and air to identify the air–water interface.

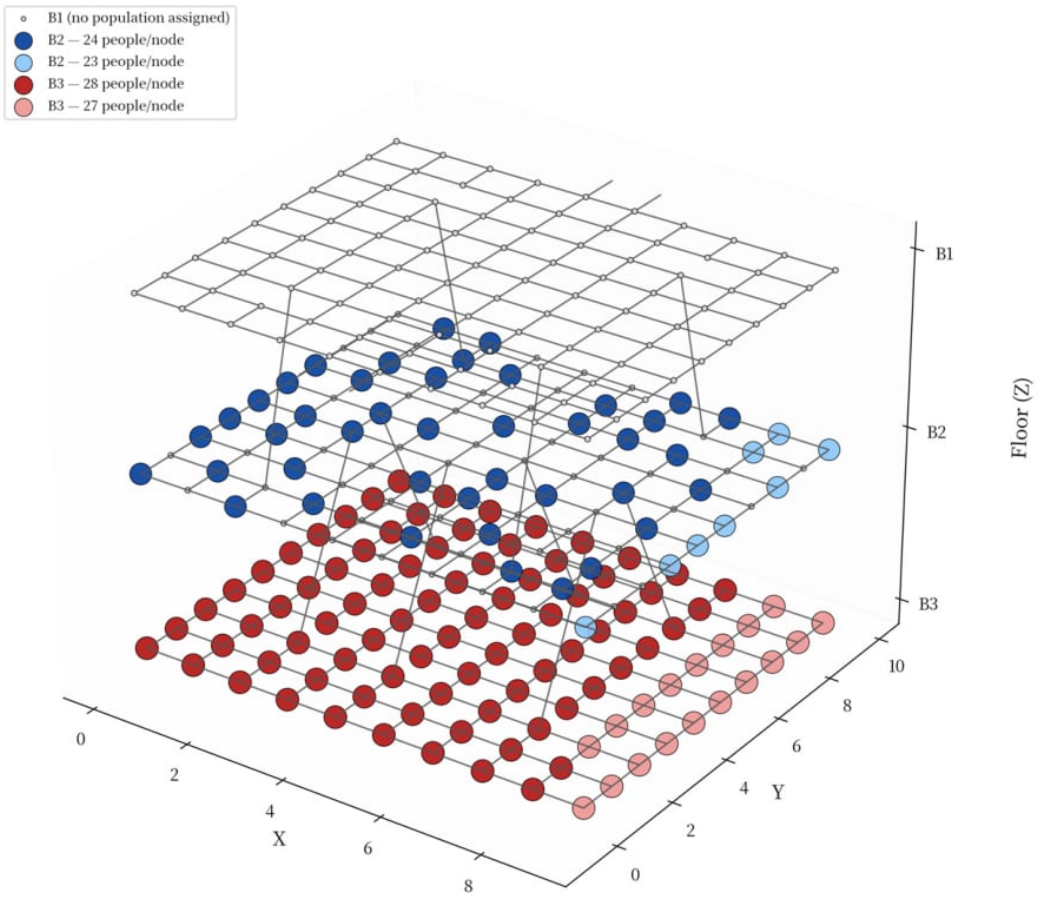

Figure 2. Node–link network of the target station with the initial occupant distribution (B3: 28/27 persons per node; B2: 24/23 persons per node on half of the concourse nodes; B1: none).

For the incompressible air–water mixture, conservation of mass is expressed by the continuity equation, while momentum conservation is governed by the transient Reynolds averaged Navier–Stokes equations. Turbulence was modeled with the Reynolds-averaged k-ω SST with the coefficients of the OpenFOAM implementation based on Menter [21]. This model combines near-wall performance of the k-ω formulation with the free-stream characteristics of the k-ε approach and is suitable for flows involving strong velocity gradients and complex structure conditions. These characteristics are particularly relevant to staircase flooding, where flow accelerates along inclined surfaces and undergoes abrupt directional changes near floor connections. The hydraulic simulation was continued for 600 s for each entrance configuration.

Three-dimensional OpenFOAM results were subsequently post processed to obtain depth and velocity which formed the basis for calculating flood induced walking speed retention factors. The simulated water depth and velocity were used to estimate inundation related reductions in pedestrian walking speed following the experimental results by Ishigaki et al. [22] as:

$$V_{rc} = 0.45e^{-120M} - 0.85M + 0.55 \quad (1)$$

$$V_{rs} = 0.15e^{-100M} - 0.8M + 0.85 \quad (2)$$

$$M = \frac{h^2}{2} + \frac{hU^2}{g} \quad (3)$$

where V_{rc} and V_{rs} are the walking speed retention factors for corridors and stairways, respectively; M is the specific force per unit width (m^3/m); h is the inundation depth (m); U is the flow velocity (m/s); g is the gravitational acceleration (m/s^2). The calculated

walking speed reduction rates were used to determine the link weights in the evacuation route selection algorithm.

The computational domain was initially dry, and a constant volumetric inflow rate was prescribed at each unprotected entrance. Entrances protected by flood barriers were represented as impermeable walls. The outlet on B3 and the air openings above the entrances were represented as open boundaries. At these boundaries, a total-pressure boundary condition was prescribed, together with a velocity boundary condition permitting outflow and reverse inflow. A zero-gradient boundary condition for turbulence were used at the B3 outlet. Walls used a non-slip condition for velocity and wall functions used for the near-wall turbulence treatment. Previous work [4] evaluated predictions of inundation depth using this model with point-gauge measurements at three sections of a 1:20 laboratory subway station model. The mean absolute percentage errors were 7.02% and 7.55% for the two tested discharges. These measurement comparisons support the use of the modeling approach for flooding subway simulations.

2.4. Evacuation Simulation Model

Evacuation routing was modeled with Dijkstra's algorithm [10] on a node–link representation of the station, in which nodes correspond to 5 m × 5 m cells of the platform, concourse and exit levels and links represent the walkable connections between them. Each link carries a weight equal to its travel time, obtained from the link length and the walking speed applicable to that link. Starting from an origin node, the algorithm repeatedly selects the unvisited node with the smallest cumulative cost, updates the cost of its neighbors whenever a shorter path is found, and terminates when every reachable node has been finalized (Figure 3). Because the search is exhaustive rather than heuristic, it returns the globally shortest path for any non-negative weight configuration, which is the property required here: the link weights change during the simulation, and an approximate search could miss a route that becomes optimal only after congestion or flooding has altered the costs.

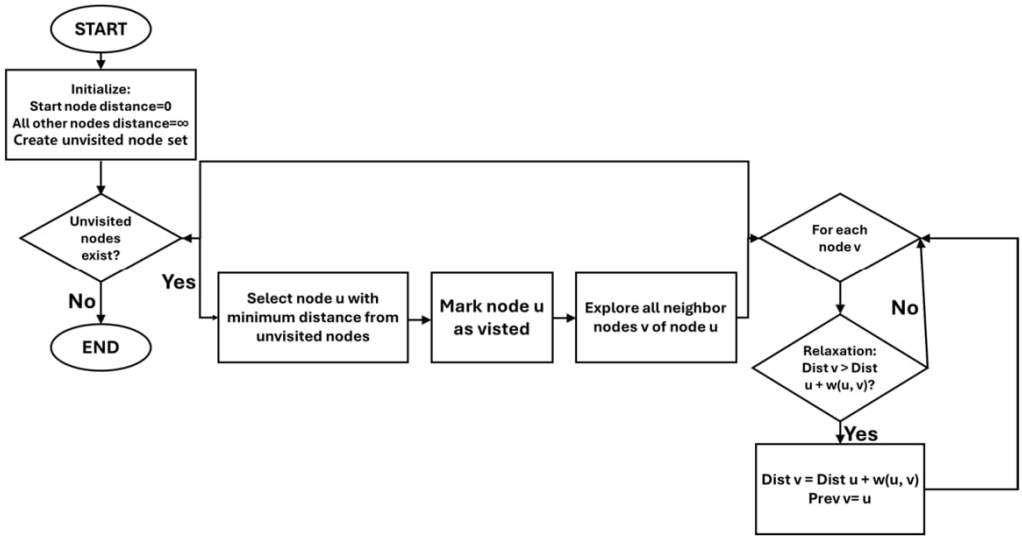

Figure 3. Dijkstra's Algorithm Flow Chart [10].

Baseline walking speeds of 60 m/min on horizontal links and 15 m/min on stairway links were adopted from the MOLIT design guidelines for urban railway stations [23] and applied to all evacuees. The low stairway value allows for elderly and mobility-impaired passengers. Escalators were assigned the stairway speed, since their power supply is assumed to be shut off once flooding begins.

Crowding was introduced as a speed reduction applied to any link whose connecting node exceeds a prescribed occupancy threshold. The reduction factors were determined from the density–speed relationship of Zhou et al. [9], derived from video observation of evacuating pedestrians, in which walking speed decreases nonlinearly with density and approaches a lower bound at high densities (Figure 4). The relationship was discretized into three tiers corresponding to nodal densities of 1, 2 and 3 persons/m^2, i.e., 25, 50 and 75 persons for the 25 m^2 node, with the link weight multiplied by 2, 2.5 and 3, respectively (Table 2). Each multiplier was taken conservatively from the upper end of its density range, so that the walking speed within a congested node is reduced to roughly one half, two fifths and one third of the free-flow value as density increases.

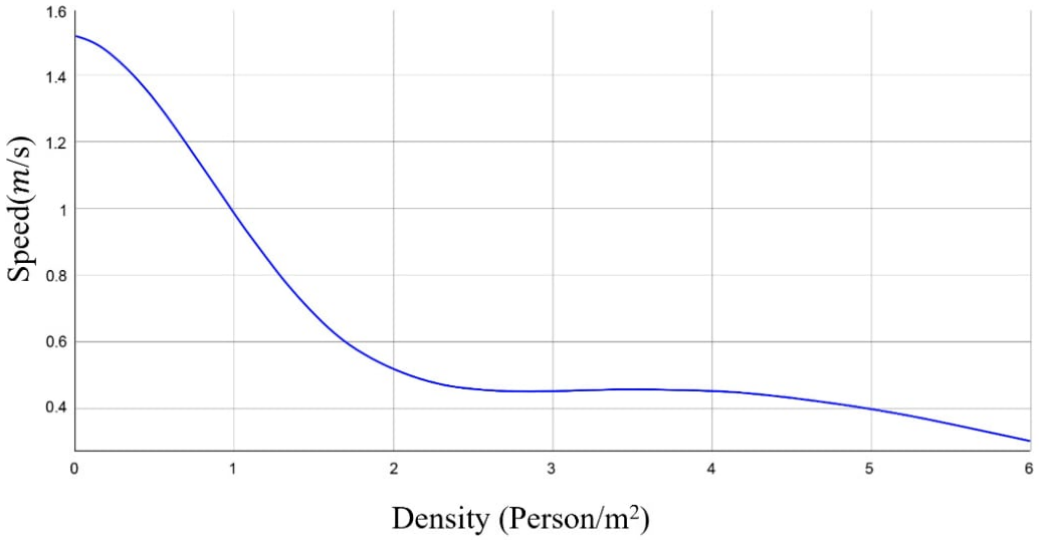

Figure 4. Density–speed relationship for pedestrian evacuation [9].

Table 2. Congestion thresholds and speed reduction multipliers applied to link weights.

Nodal Occupancy Threshold (Persons)	Nodal Density (Persons/m^2)	Speed Reduction Multiplier
25	1	2
50	2	2.5
75	3	3

The evacuation was computed with the following procedure. First, the 3974 occupants were assigned to the platform and concourse nodes as described above, with the same random selection of concourse nodes used in all cases. Second, each link i–j was given a travel time cost $t_{ij} = L_{ij}/(v_0 \cdot V_{r,ij}) \times C_j$, where L_{ij} is the link length (5 m for horizontal links and 5 m along the incline for stairway links), v_0 is the baseline walking speed, $V_{r,ij}$ is the flood-induced walking speed retention factor and C_j is the congestion multiplier of the downstream node j. The retention factor was evaluated node by node from the depth and velocity averaged over the CFD cells within each 5 m × 5 m node, using Equation (1) for horizontal links and Equation (2) for stairway links. Third, at every time step of $\Delta t = 1$ s, Dijkstra's algorithm was solved from every occupied node to the entrances on the current costs, and the occupants of each node were advanced along the first link of their shortest path. Fourth, the nodal occupancies were updated, the congestion multipliers were reassigned according to Table 2, and the procedure was repeated until all occupants had evacuated. An occupant was counted as evacuated on arrival at an entrance node on the exit level, and this arrival time was recorded as the occupant's evacuation time. The maximum evacuation

time is the arrival time of the last occupant, and the mean evacuation time is the arithmetic mean of the individual evacuation times of all 3974 occupants. Because the inputs and the occupant distribution were fixed, the model is deterministic and each case was run once. The key parameters are listed in Table 3.

Table 3. Key parameters of the evacuation model.

Item	Value
Node size	5 m × 5 m (25 m^2)
Number of nodes	B3: 100, B2: 100, B1: 100
Link length	5 m (horizontal), 5 m along the incline (stairway)
Baseline walking speed	60 m/min (horizontal), 15 m/min (stairway and escalator)
Flood-induced speed retention	Equations (1) and (2), evaluated per node
Congestion thresholds and multipliers	25/50/75 persons → 2/2.5/3
Time step and path update	1 s, path re-solved every time step
Available exits	Four entrances in all cases
Population	3974 (B3: 2782, B2: 1192)
Evacuation criterion	Arrival at an entrance node on the exit level

Flood barriers were treated as obstacles to water but not to pedestrians, so all four entrances remained available as exits in every case. An entrance flood barrier acts as a raised sill across the entrance that blocks surface water while evacuees can still pass over it. If a protected entrance could not be used, each barrier would also remove an exit from the network, and the evacuation benefits reported here should therefore be regarded as an upper bound.

The cases differ in a single input to the evacuation model. The water depth and flow velocity obtained from the inundation simulation of each case were converted into walking-speed reduction factors and applied to the links of the affected nodes as a fixed spatial input for that case; this component represents the inundation state associated with a given barrier configuration and was held constant during the evacuation run. The congestion component, in contrast, was recalculated at every time step from the evolving nodal occupancy, and the shortest path from each occupied node to the nearest entrance was re-solved on the updated weights. The network geometry, the set of available entrances, the initial occupant distribution and the congestion parameters were identical in all cases, so that any difference in evacuation performance reflects the change in inundation produced by the barriers.

3. Simulation Results

3.1. Inundation Simulation Results

To represent a hypothetical inundation scenario for underground inundation, a constant overflow depth of 0.2 m was assumed above the top of the entrance stairway for 10 min. The inflow discharge was calculated using the overflow equation proposed by Nakasaka and Ishigaki [24]:

$$Q = C_d b \sqrt{g} H^{1.5} \quad (4)$$

where Q is the inflow discharge (m^3/s); $C_d = 0.85$ is the discharge coefficient; b is the entrance-stair width (2.0 m), H is the overflow depth above the top of the stairway (0.2 m).

To examine sensitivity to spatial resolution, the configuration with all entrances open was repeated on a coarser and a finer mesh with approximately half and twice the number of cells of the original mesh, corresponding to refinement ratios of 1.25 and 1.28 in each direction with all other settings were unchanged. The mean water depths on the coarse, original and fine meshes were 0.223, 0.257 and 0.259 m on B1, 0.086, 0.112 and 0.113 m on B2, and 0.038, 0.044 and 0.043 m on B3. Between the original and fine meshes, mean

depths differed by less than 3%, showing mesh independence. The research also tested mesh independence in the stairway, which reached velocity values of 7.5, 5.4, 4.8, 4.8 m/s, with refinement ratios of 2, 3, 4, in which the 3 and 4 refinement ratio lead to the same results which were then used for further simulations. To find time-step sensitivity, a test was performed by halving the Courant number from 1 to 0.5 for the all-entrances-open case. The mean water depths on B1, B2 and B3 changed by −1.3%, +0.9% and −1.8%, and the total water volume in the station by 1%. The results are therefore insensitive to the time step, and the Courant number of 1 was used for all simulations.

Figures 5 and 6 presents the spatial distribution of simulated water depth and depth-averaged velocity within the three level underground station at t = 600 s. Figure 5 shows the water depth on the three floors at t = 600 s for the different barrier configurations. With all four entrances open (Figure 5a), the water was deepest on B1 with a mean value of 0.26 m, decreased to about 0.11 m on B2 and to about 0.04 m on B3. Closing entrances reduced the depth on every floor, with the B1 level falling to 0.2 m for three open entrances (Figure 5b), 0.14 m for two (Figure 5c,d) and 0.07 m for one (Figure 5e,f). For the same number of open entrances, the depth fields are nearly identical regardless of which entrances remained open, showing that the number of open entrances governs the flooding depth.

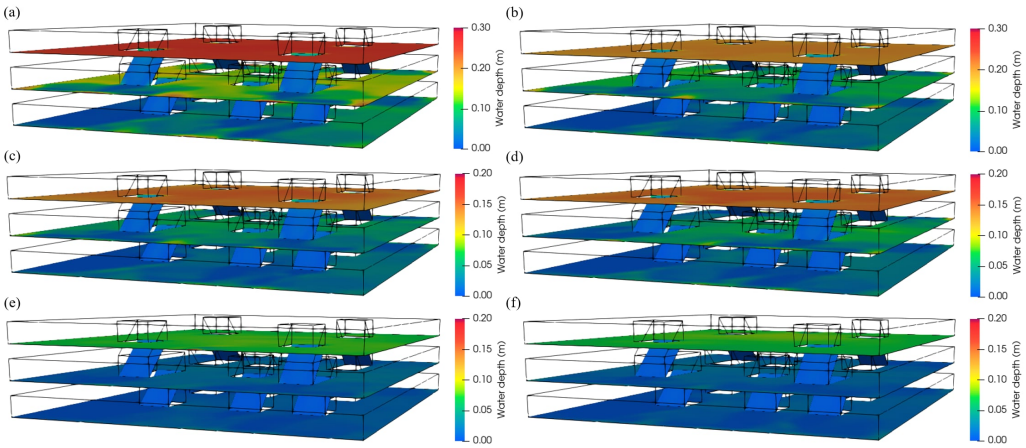

Figure 5. Simulation results of water depth: (**a**) 0 flood barriers closed; (**b**) 1 flood barriers closed; (**c**) 2 flood barriers closed1; (**d**) 2 flood barriers closed2; (**e**) 3 flood barriers closed1; (**f**) 3 flood barriers closed2.

Across all six barrier configurations, relatively low velocities prevailed over the horizontal floors, while higher velocities were concentrated along the inter-floor stairways and the jets emerging from their downstream ends shown in Figure 6. Across the sampled B1 grid locations, the mean velocities were 0.190 m/s, 0.177 m/s, 0.151 m/s, and 0.165 m/s for the 0, 1, 2, and 3 flood barrier closed scenarios, respectively. On B2 and B3, the descending stairway flows formed narrow jets that spread across the receiving floors. The mean stairway velocities ranged from 4.4 to 4.7 m/s between B1 and B2 and from 4.3 to 4.8 m/s between B2 and B3. On B2 and B3, high velocity flows extended from the lower ends of the stairways into the surrounding floor areas, with velocities generally decreasing laterally away from these flows. The median velocities ranged from 0.43 to 0.60 m/s on B2 and from 1.18 to 1.26 m/s on B3. This is consistent with flow acceleration during stairway descent and the spreading of concentrated flow over the receiving floor. From the barriers, a reduction in incoming water volume did not necessarily correspond to a reduction in local velocity along the remaining flow pathways.

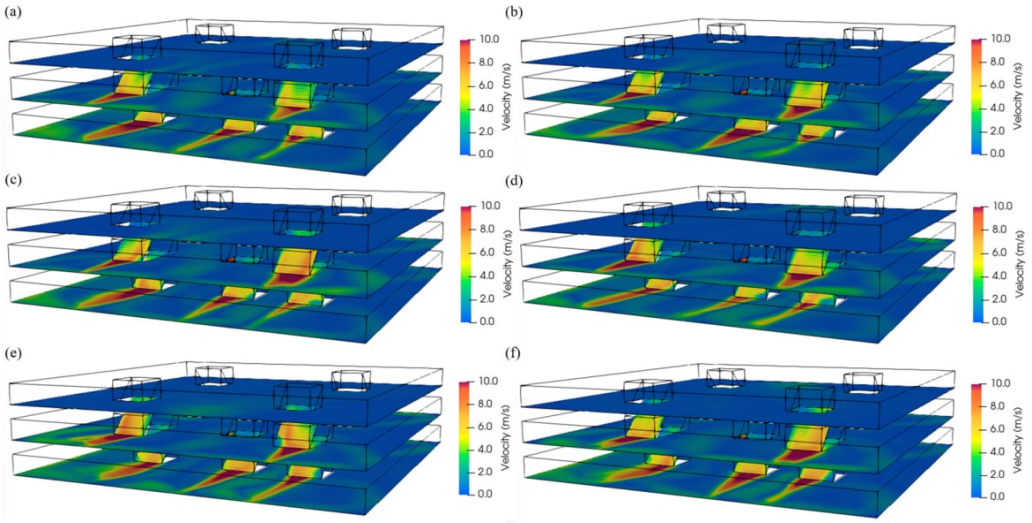

Figure 6. Simulation results of flow velocity: (**a**) 0 flood barriers closed; (**b**) 1 flood barriers closed; (**c**) 2 flood barriers closed1; (**d**) 2 flood barriers closed2; (**e**) 3 flood barriers closed1; (**f**) 3 flood barriers closed2.

To find the effect of barrier placement, Figure 5d,f and Figure 6d,f was compared depicting 1 open and 2 open barriers at different locations. For flooding effect of barrier placement, the mean depths differ by at most 0.002 m, walking-speed factors by at most 0.011, and stored volume by under 0.2%. The only local difference was shown near the open entrances. Therefore, barrier placement has a negligible effect on depth, velocity and walking-speed factors. Inundation was governed by the number of protected entrances through the total inflow, not the barrier position.

These results show that increasing entrance protection did not produce a uniform reduction in local velocity, particularly along the flow pathways connecting the lower levels. The velocity fields indicate that the entrance closure configurations with flood barriers modify the distribution of hydraulic loading among the inter floor connections rather than producing a uniform reduction in local velocity. For evacuation modeling, this spatial variability requires stairway specific hydraulic inputs, as a low velocity over much of a floor does not necessarily imply favorable conditions along the stairways needed to reach the surface. Therefore, walking speed reduction should consequently be evaluated using the local velocity together with the corresponding water depth.

The hydraulic results were subsequently converted into pedestrian walking speed factors and visualized as the percentage of normal walking speed retained under each flood barrier scenario shown in Figure 7. For each scenario the walking speed factors were spatially averaged so that it could be used as factors for speed reduction which would be used in the node-link network in the evacuation model. Under the 0-closed baseline, the mean pedestrian-speed retention over the valid horizontal cells was approximately 52.7% on B1, 63.5% on B2, and 76.2% on B3, corresponding mean water depths 0.257 m on B1, 0.111 m on B2, and 0.040 m on B3. The strongest reduction therefore occurred on the upper level, where floodwater first entered, although several localized areas on B2 and B3 also showed severe impairment. The B1–B2 stairways were particularly affected, with an average equivalent to a reduction of about 49.4%.

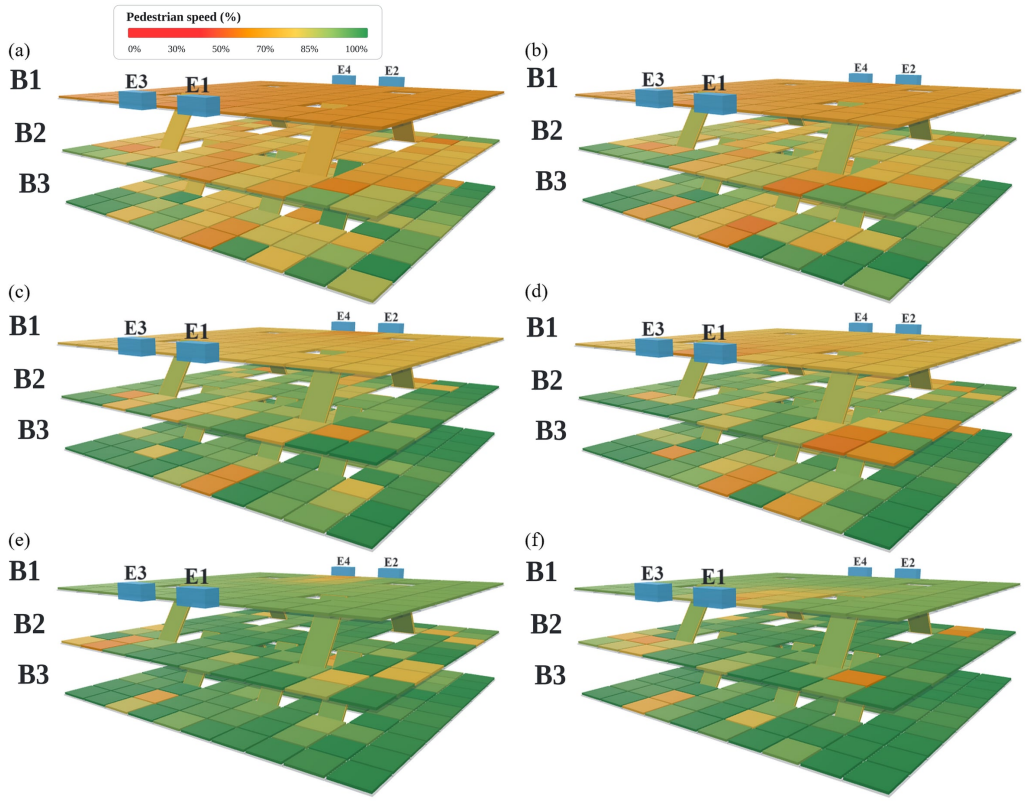

Figure 7. Pedestrian speed changes: (**a**) 0 flood barriers closed; (**b**) 1 flood barriers closed; (**c**) 2 flood barriers closed1; (**d**) 2 flood barriers closed2; (**e**) 3 flood barriers closed1; (**f**) 3 flood barriers closed2.

As additional water entrances by flood barrier were closed, pedestrian mobility progressively improved. For the 2-closed case, the mean retained speed increased to approximately 65.7% on B1, 80.8% on B2, and 86.5% on B3. The greatest difference occurred in the 3-closed case, for which the corresponding values increased to approximately 85.7%, 89.1%, and 90.0%, giving average reductions walking speed of only about 14.3%, 10.9%, and 10.0%. The mean retained speed on the B1–B2 stairs also increased to approximately 79.2%, compared with 50.6% in the baseline case. These results indicate that entrance closure improves pedestrian mobility not only near the protected entrances but also along downstream inter floor connections. Nevertheless, the nonuniform velocity field means that individual stairways may remain locally unfavorable even when overall flooding is reduced, emphasizing the importance of using spatially distributed walking speed values rather than a single floor-averaged reduction factor when constructing the subsequent evacuation routing model.

Overall, the results show a clear reduction in mobility impairment as the number of closed entrances increases, but the change was shown to be spatially nonlinear. This behavior is consistent with the former observations that hydraulic conditions can vary significantly within the same underground level, and that flood induced mobility reduction is related to the available inter floor flow pathways. The results further display that these localized hydraulic differences are important because they directly modify the speed assigned to links in the evacuation simulation.

3.2. Evacuation Simulation Results

Table 4 summarizes the maximum and mean evacuation times for the six barrier configurations. Without a flood barrier (Case 1), evacuation of the 3974 occupants was completed in 574 s. A barrier at one entrance (Case 2) reduced the maximum evacuation time to 542 s, a reduction of 5.6%. With two barriers the time was 468 s and 487 s for the

two placements (Cases 3 and 4), and with three barriers 400 s and 399 s (Cases 5 and 6), corresponding to reductions of 15.2–18.5% and 30.3–30.5%. The mean evacuation time decreased from 410.0 s in Case 1 to 295.3–295.7 s in Cases 5 and 6. All four entrances remained available for evacuation in every case, so these differences reflect the change in inundation rather than a change in the number of exits.

Table 4. Maximum and mean evacuation times for each flood barrier configuration.

Case	Number of Entrances with Flood Barrier	Maximum Evacuation Time (s)	Change Relative to Case 1	Mean Evacuation Time (s)
1	0	574	–	410.0
2	1	542	−5.6%	384.7
3	2 (placement 1)	468	−18.5%	336.9
4	2 (placement 2)	487	−15.2%	343.8
5	3 (placement 1)	400	−30.3%	295.3
6	3 (placement 2)	399	−30.5%	295.7

The reduction was not proportional to the number of barriers. The first barrier shortened the maximum evacuation time by 32 s, the second by a further 55–74 s and the third by a further 68–88 s, depending on placement. This follows from the form of the walking speed retention factor, which decreases steeply with the specific force at small depths and velocities but only gradually at larger ones. While the inundation on the exit and concourse levels remains in the range where the factor varies slowly, removing a quarter of the inflow improves the walking speed on the inundated links only slightly. As further barriers bring the depth and velocity toward the range where the factor varies steeply, the second and third barriers yield larger gains than the first.

Placement affected the result with two barriers but hardly with three. The two two-barrier configurations had nearly identical floor-averaged depths and walking speed factors, yet their maximum evacuation times differed by 19 s, whereas the two three-barrier configurations differed by only 1 s. The mean evacuation times of the two two-barrier configurations differed by only 6.9 s, so the difference is concentrated in the last occupants. Because the walking speed factors were applied node by node, the local differences in depth and velocity near the open entrances, where the remaining inflow enters and the last occupants converge, were carried into the evacuation model. With two open entrances these local differences lie on the routes of the governing occupants. With three barriers the inflow through the single open entrance is small, and the local difference has little effect.

Figure 8 shows the route of the last occupant in each case. In every case this occupant starts on the platform level and climbs through the concourse to the exit level. In Case 1 the last occupant leaves through a different entrance from Cases 2–6, in which the last occupant leaves through the same entrance. The routes differ mainly in their lateral detours on the concourse and exit levels, where the algorithm steers the occupant around nodes crowded by other evacuees converging on the same stairways. These detours are congestion avoidance rather than a response to water. Cases 5 and 6 follow clearly different routes yet finish within 1 s of each other, and the route shapes do not follow the order of the evacuation times. The trend in Table 4 is therefore governed by the walking speed on the inundated links, that is, by how much the barriers reduce the depth and velocity inside the station, rather than by the route.

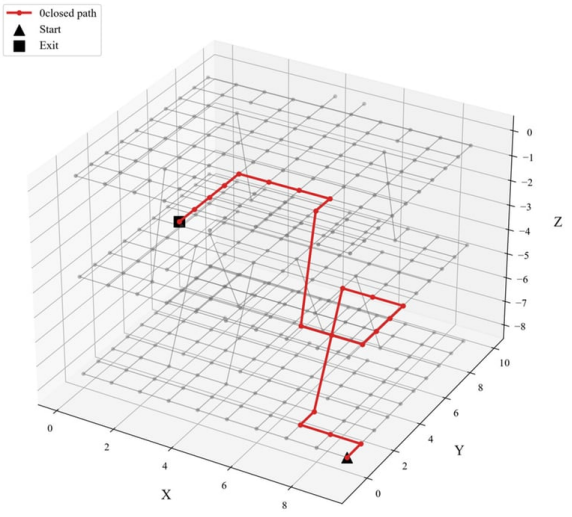

(**a**)

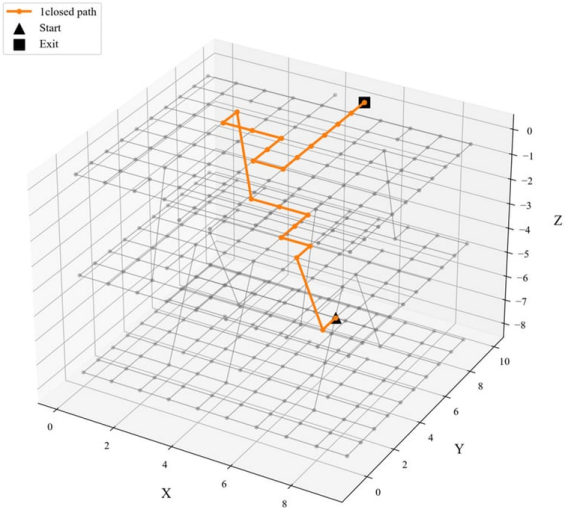

(**b**)

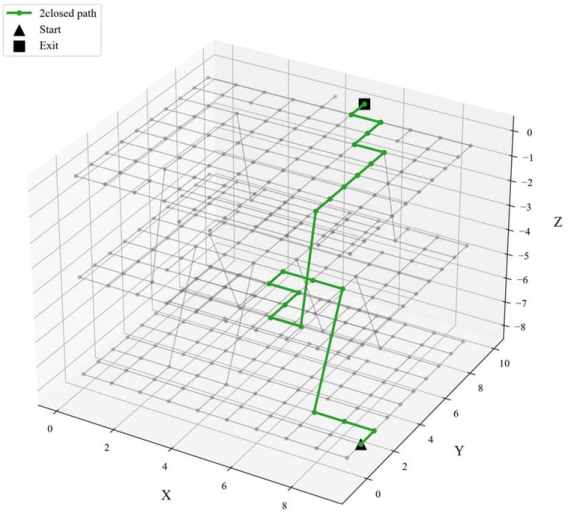

(**c**)

Figure 8. *Cont.*

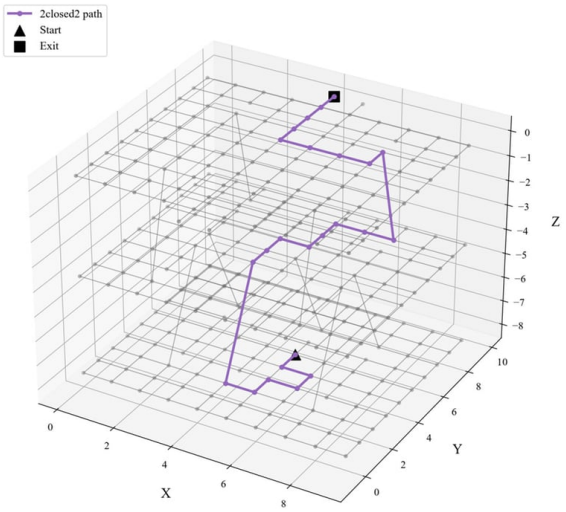

(**d**)

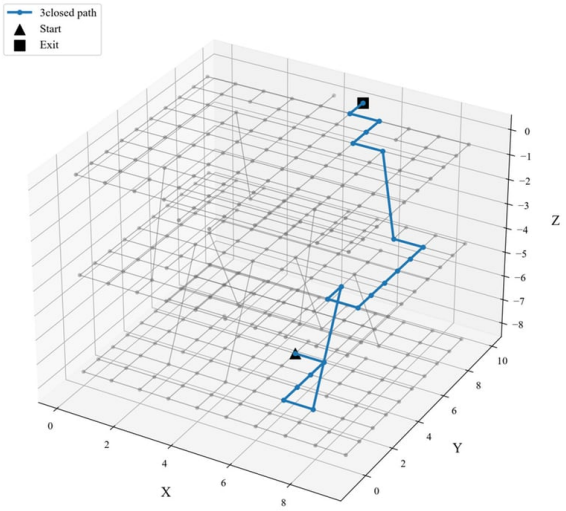

(**e**)

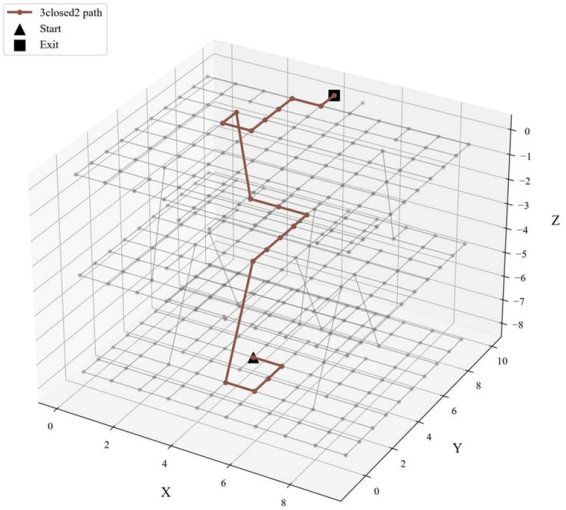

(**f**)

Figure 8. Route of the last evacuated occupant for (**a**) Case 1, (**b**) Case 2, (**c**) Case 3, (**d**) Case 4, (**e**) Case 5 and (**f**) Case 6.

4. Discussion

The hydraulic simulations indicate that flood propagation within the station was strongly controlled by the stairways connecting successive underground levels. Relatively low velocities over broad horizontal floor areas coexisted with concentrated high velocity flow along the inclined connections and immediately downstream of their outlets. This pattern reflects the acceleration of floodwater as it descends the stairs and spreads across the receiving floors. Elevated velocities downstream of several stairways suggest that these connections affected flow beyond the stair outlets, creating substantial velocity differences within the same floor. It was shown that a single floor-averaged velocity therefore does not characterize the inundation field. The three-dimensional simulation captures how descending stairway flow spreads across the receiving floors. It provides local water depths and velocities for assessing inundation on each floor and flow conditions at connections between floors.

The influence of entrance flood barriers reflects the interaction between the imposed reduction in inflow and the internal distribution of water through the station. Under identical prescribed discharge conditions at the four entrances, protecting one, two, and three entrances would reduce total inflow by 25%, 50%, and 75%, respectively. However, these boundary condition reductions need not produce proportional changes in local depth or velocity because the remaining inflow is distributed between temporary storage on each floor and discharge through the floor connections. High-velocity regions weakened on some B1–B2 stairways but persisted at other B1–B2 and B2–B3 connections, indicating an uneven hydraulic response. An unprotected entrance may continue to supply a particular stairway even as inflow to other areas decreases. Furthermore, reduced stairway discharge may be accompanied by a smaller wetted cross-sectional area, allowing relatively high velocities to persist despite a reduction in the volume of water conveyed. High velocities may persist at specific locations even when flood barriers reduce the overall volume and depth of water within the station. Therefore, barrier effectiveness should instead be evaluated using the combined changes in water depth, flow velocity, and discharge along the remaining hydraulic pathways.

The prescribed overflow depth of 0.2 m maintained for 600 s provides a controlled basis for comparing barrier configurations, but limits the interpretation of the results under actual flood conditions. Although the internal flow was simulated transiently, the constant results used for the speed reduction calculation does not represent the rising and falling stages of a surface flood or the redistribution of surface water toward unprotected entrances. Water depth may continue to increase in low velocity floor areas while concentrated stairway flows persist, meaning that velocity maps alone cannot establish the final extent or severity of inundation. The results therefore describe the station's hydraulic response at the examined simulation stage under controlled entrance conditions. Future analysis could use time varying entrance hydrographs and examine how the timing of barrier installation affects surface water redistribution. Time series of water storage and discharge for each floor could further clarify how barrier configurations influence the timing and magnitude of underground inundation.

From the evacuation side, the benefit of flood barriers appears as a change in walking speed rather than as a change in route. Configurations with clearly different routes for the last occupant reached nearly the same evacuation time, while the evacuation time decreased steadily as the inundation was reduced. What changes between the cases is the depth and velocity of water on the links of the concourse and exit levels, and hence the speed penalty applied to those links. In a station of this type, the effectiveness of a barrier scheme for evacuation can therefore be judged largely by how much it reduces inundation in the

circulation areas above the platform, a hydraulic quantity that can be estimated before an evacuation simulation is run.

The benefit was not proportional to the number of barriers: the first barrier shortened the maximum evacuation time by 32 s, whereas the second and third each shortened it by a further 55–88 s. Partial installation therefore yields a smaller benefit per barrier than protection of most entrances. Where the number of barriers is limited by cost or by the need to keep entrances open, priority should go to the entrances that contribute most to the inflow reaching the concourse.

Placement had a measurable effect when two entrances were protected. The two configurations produced nearly the same floor-averaged inundation but differed by 19 s in maximum evacuation time, about 3% of the no-barrier value, because the local inundation near the open entrances lay on the routes of the last occupants. In Cases 2–6 the last occupant left through the same entrance regardless of placement, indicating that the binding congestion forms on that side of the station because of the position of the stairways relative to the initial occupant distribution. The absolute evacuation times and the governing exit thus depend on the relative positions of the entrances, stairways and occupants, and would differ in a station with another layout. The mechanisms identified here are that barriers act through walking speed rather than route, that the benefit grows more than proportionally with the number of barriers, and that placement matters most when inundation is moderate. These mechanisms arise from the form of the walking speed relationship and from the role of stairways as common pathways for water and evacuees, which most multilevel stations share. They are therefore expected to carry over to other layouts, whereas the numerical values require analysis of the actual station geometry. Real-time guidance that directs part of the platform population toward less crowded entrances from the outset would be the operational counterpart of the rerouting observed in the simulation.

Several simplifications should be kept in mind when interpreting these results. The inundation field was fixed for each case, so the analysis represents a snapshot of flood progression rather than an evolving hazard. All occupants were assigned the same baseline walking speeds, although elderly people, children and passengers with luggage walk more slowly and are more strongly affected by water. Congestion was represented by three discrete tiers on a 25 m^2 node, which captures the order of magnitude of the speed loss but produces step changes at the thresholds. The population was taken from the peak 30-min boarding volume, an upper bound on the simultaneous occupancy, and was divided between the platform and the concourse in a fixed 7:3 ratio. In every case the concourse occupants left the station first, with mean evacuation times of 190.5–273.9 s, and the last occupant was always a platform occupant, the platform occupants having mean evacuation times of 338.5–468.2 s. With this ratio the platform nodes start in the first congestion tier and the concourse nodes just below it. The platform remains in the first tier for any platform share above 63%, whereas the concourse enters it once its share exceeds about 31%. A larger concourse share would therefore add initial congestion on the concourse, while a smaller one would leave the initial congestion state unchanged. Protected entrances were assumed to remain passable; if they could not be used, each barrier would also remove an exit and the benefits reported here would be reduced. These assumptions were applied identically to all cases, so the comparison between configurations is less affected than the absolute evacuation times.

Also, the findings are restricted to the idealized station geometry, the prescribed entrance forcing and the six barrier configurations examined. Because the number and location of protected entrances changed together, the calculated differences cannot establish a general relationship between barrier count and evacuation benefit or identify an optimal barrier arrangement. Application to an operating subway station would require actual geome-

try, verified hydraulic boundary conditions, and validation with evaluation of evolving inundation and pedestrian access through protected entrances.

5. Conclusions

This study used three-dimensional OpenFOAM simulations for inundation modeling with a Dijkstra-based evacuation model to assess six cases of entrance flood barriers in an ideal three level underground subway station. Spatially distributed water depth and depth-averaged velocity were converted into pedestrian walking speed retention factors and applied to evacuation links, while nodal congestion was updated during the evacuation of 3974 occupants. The research connected changes in entrance protection to local hydraulic conditions and the resulting station evacuation.

Entrance protection improved estimated pedestrian mobility throughout the station, although localized speed reduction remained near inter-floor connections. The hydraulic results showed spatially heterogeneous mobility reduction, with concentrated flow along inter-floor stairways. Between the unprotected and three-barrier configurations, mean walking speed retention increased from 52.7% to 85.7% on B1, from 63.5% to 89.1% on B2, and from 76.2% to 90.0% on B3. The corresponding increase on the B1–B2 stairways was from 50.6% to 79.2%. Maximum evacuation times were 574 s with no barrier, 542 s with one, 468–487 s with two and 399–400 s with three, depending on placement. Three barriers produced the shortest evacuation time, reducing the baseline by up to 175 s, or 30.5%. The first barrier reduced the evacuation time by 5.6%, and the second and third barriers gave larger reductions, so the effect was not proportional to the number of barriers. The benefit of flood barriers appeared as a change in walking speed rather than as a change in route.

These results are subject to the limitations of the analysis. The station geometry was idealized, so the absolute evacuation times and the governing exit depend on the assumed positions of the stairways and entrances; the 19 s difference between the two two-barrier configurations, which had nearly identical inundation, indicates the extent of this dependence. The inundation field was fixed for each configuration and did not evolve during evacuation. Evacuation was represented with uniform design walking speeds, three discrete congestion tiers, a single peak-ridership population, and the assumption that entrances protected by barriers remained passable for evacuees. The results are therefore intended for comparing barrier configurations under controlled conditions rather than for predicting evacuation times at a specific station.

These findings support assessing flood barriers according to the mobility conditions they preserve along evacuation routes, particularly stairways connecting underground levels. Future analysis should incorporate flood conditions that evolve during evacuation, explicitly evaluate pedestrian access through protected entrances, and test more alternative barrier locations. Such research would further clarify how the effects of flood barriers observed here depend on flood timing and exit availability.

Author Contributions: C.Y.K.: Writing—original draft, methodology., J.S.: Writing—review and editing, methodology, visualization. D.S.R.: Writing—review and editing, methodology. All authors have read and agreed to the published version of the manuscript.

Funding: The research for this paper was supported by KICT Research Program (Project no. 20260161–001, Development of Digital Urban Flood Control Technology for the Realization of Flood Safety City) funded by the Ministry of Science and ICT.

Data Availability Statement: The original contributions presented in this study are included in the article. Further inquiries can be directed to the corresponding authors.

Conflicts of Interest: The authors declare no conflicts of interest.

References

1. Son, A.-L.; Kim, B.; Han, K.-Y. A simple and robust method for simultaneous consideration of overland and underground space in urban flood modeling. *Water* **2016**, *8*, 494. [CrossRef]
2. Zhang, D.-M.; Li, H.-Y.; Zhou, W.-D.; Chen, S.-R.; Huang, Z.-K. A multi-layer coupling framework for hydrodynamic simulation of underground station flooding. *Tunn. Undergr. Space Technol.* **2026**, *168*, 107208. [CrossRef]
3. Liang, C.; Guo, K.; Guan, M. Computational hydraulics and hazard assessment of flooding on underground staircases. *Tunn. Undergr. Space Technol.* **2024**, *144*, 105511. [CrossRef]
4. Shin, J.; Rhee, D.S.; Park, I. Analysis of inundation flow characteristics and risk assessment in a subway model using flow simulations. *Appl. Sci.* **2024**, *14*, 8096. [CrossRef]
5. Lu, J.; Lin, Z.; Lin, H. Numerical analysis of flood invasion path and mass flow rate in subway stations under heavy rainfall conditions. *Appl. Sci.* **2024**, *14*, 7497. [CrossRef]
6. Wang, M.; Chen, G.; Liu, W.; Cui, C. Numerical simulation and disaster prevention strategies for flood intrusion process in subway stations. *Int. J. Disaster Risk Reduct.* **2024**, *114*, 104984. [CrossRef]
7. Li, Q.; Xia, J.; Xie, Z.; Zhou, M.; Deng, S. Hazard and vulnerability in urban inundated underground space: Hydrodynamic analysis of human instability for stairway evacuation. *Int. J. Disaster Risk Reduct.* **2022**, *70*, 102754. [CrossRef]
8. Helbing, D.; Farkas, I.; Vicsek, T. Simulating dynamical features of escape panic. *Nature* **2000**, *407*, 487–490. [CrossRef] [PubMed]
9. Zhou, J.; Li, S.; Nie, G.; Fan, X.; Xia, C. Developing a revised social force model for pedestrians' earthquake emergency evacuation. *Geomat. Nat. Hazards Risk* **2020**, *11*, 335–356. [CrossRef]
10. Dijkstra, E.W. A note on two problems in connexion with graphs. *Numer. Math.* **1959**, *1*, 269–271. [CrossRef]
11. Li, Z.Y.; Tang, M.; Liang, D.; Zhao, Z. Numerical simulation of evacuation in a subway station. *Procedia Eng.* **2016**, *135*, 616–621. [CrossRef]
12. Mirahadi, F.; McCabe, B.Y. EvacuSafe: A real-time model for building evacuation based on Dijkstra's algorithm. *J. Build. Eng.* **2021**, *34*, 101687. [CrossRef]
13. Zhou, M.; Dong, H.; Ioannou, P.A.; Wang, F.Y. Crowd evacuation with multi-modal cooperative guidance in subway stations: Computational experiments and optimization. *IEEE Trans. Comput. Soc. Syst.* **2022**, *10*, 2536–2545. [CrossRef]
14. Zhu, Y.; Zhou, Z.; Zhou, J.; Xu, X.; Wu, X.; Nie, W. An improved 3D Dijkstra algorithm of evacuation route considering tailings dam failure. *Nat. Hazards* **2025**, *121*, 2483–2505. [CrossRef]
15. Gonzales, S.H.; Vega-Huerta, H.; Maquen-Niño, G.L.E.; De-la-Cruz-VdV, P.; Moquillaza-Henríquez, S.D.; Benito-Pacheco, O.; Cabrera-Diaz, J.; Lázaro-Guillermo, J.C. Optimized earthquake evacuation routes using Dijkstra's algorithm and WinQSB. *J. Comput. Sci.* **2025**, *21*, 2349–2360. [CrossRef]
16. Haam, S.; Kim, H.; Yoo, M.; Song, W.S. Optimal additional evacuation route analysis in deep underground station structures using Dijkstra's algorithm. *Dev. Built Environ.* **2025**, *24*, 100784. [CrossRef]
17. Kim, H.; Haam, S.; Yoo, M.; Song, W.S. Algorithmic evaluation of fire evacuation efficiency under dynamic crowd and smoke conditions. *Fire* **2026**, *9*, 32. [CrossRef]
18. Haam, S.; Kang, C.; Kim, H.; Yoo, M. Centralized exit allocation framework for system optimal evacuation in underground stations. *Dev. Built Environ.* **2026**, *27*, 100967. [CrossRef]
19. Hou, J.; Chen, G.; Zhang, Y.; Li, B.; Yang, S.; Tong, Y.; Zhang, D.; Fu, D. A simulation study on risks of pedestrian evacuation from flooded staircases of different slopes in the underground space. *Nat. Hazards* **2022**, *110*, 519–543. [CrossRef]
20. Lin, Z.; Hu, S.; Lin, H. Flow pattern and escape hazards of people from flood intrusion into the staircase of underground spaces with multiple rest platforms. *Buildings* **2024**, *14*, 941. [CrossRef]
21. Menter, F.R. Two-equation eddy-viscosity turbulence models for engineering applications. *AIAA J.* **1994**, *32*, 1598–1605. [CrossRef] [PubMed]
22. Ishigaki, T.; Asai, Y.; Nakahata, Y.; Shimada, H.; Baba, Y.; Toda, K. Evacuation of aged persons from inundated undergroundspace. *Water Sci. Technol.* **2010**, *62*, 1807–1812. [CrossRef] [PubMed]
23. Ministry of Land, Infrastructure and Transport (MOLIT). *Design Guidelines for Urban Railway Stations and Transfer Facilities*; Notice No. 2022-78; MOLIT: Sejong, Republic of Korea, 2022.
24. Nakasaka, Y.; Ishigaki, T. Vulnerability to mega under- ground inundation and evacuation assuming devastating urban flood. *J. Disaster Res.* **2021**, *16*, 321–328. [CrossRef]

Disclaimer/Publisher's Note: The statements, opinions and data contained in all publications are solely those of the individual author(s) and contributor(s) and not of MDPI and/or the editor(s). MDPI and/or the editor(s) disclaim responsibility for any injury to people or property resulting from any ideas, methods, instructions or products referred to in the content.